DOI: 10.61782/fa.2025.0711

FORUM ACUSTICUM EURONOISE 2025

PSYCHOACOUSTIC CHARACTERIZATION OF AN ISOLATED PROPELLER AT DIFFERENT INFLOW TURBULENCE CONDITIONS AND COLLECTIVE PITCH ANGLES

Roberto Merino-Martínez [1*] **Luca Nicola Quaroni**[1]

[1] Faculty of Aerospace Engineering, Delft University of Technology, the Netherlands

ABSTRACT

The far-field acoustic emissions of a six-bladed propeller were investigated in aeroacoustic experiments in an open-jet wind tunnel. The propeller was operating in different isotropic inflow turbulence conditions generated by turbulence grids placed upstream of the exit plane of the wind tunnel nozzle. In addition, the collective pitch angle of the propeller blades was also varied throughout the measurements. A preliminary directivity analysis of different acoustic and psychoacoustic metrics was performed to investigate the influence of the inflow turbulence intensity and collective pitch angle on the noise emissions and sound perception. In general, increasing the inflow turbulence levels did not modify the conventional metrics recorded, e.g. equivalent sound pressure level. Nevertheless, it considerably increased the broadband noise emissions of the propeller, the loudness, and the overall psychoacoustic annoyance metrics. However, notable reductions in tonality (due to partial tone masking because of the higher levels of broadband noise) and sharpness were reported for increasing turbulence intensities. Overall, this analysis is valuable for the perception-influenced design of devices equipped with propellers, such as drones or urban air mobility vehicles, to account for installation effects.

Keywords: *Propeller noise, psychoacoustics, sound quality metrics, tonality, turbulence ingestion.*

**Corresponding author*: r.merinomartinez@tudelft.nl.

1. INTRODUCTION

An increasing number of devices employ propellers, such as drones [1] and urban air mobility vehicles [2,3], as well as aerospace technologies (e.g. distributed electric propulsion [4] and boundary layer ingestion systems [5]). Therefore, during the last years, considerable research has been devoted to investigating propeller noise emissions [6, 7] and, from a psychoacoustic point of view, the corresponding human perception [8, 9]. This has led to the use of perception-influence design of propellers to cause minimal noise annoyance during operation [10].

Most aeroacoustic experiments, for simplicity reasons, feature isolated propellers (typically conducted in anechoic chambers [10, 11] or wind tunnels [7]) and consider clean, low-turbulence inflow conditions. However, in practice, the usual installation of propellers close to the airframe (e.g. on aircraft or drones) typically causes turbulent inflow conditions [12]. Despite some studies on this topic [6,13,14], there is currently a lack of knowledge on how inflow turbulence influences propeller noise emissions, especially in terms of broadband noise and sound perception.

Therefore, the present paper provides a psychoacoustic characterization (using psychoacoustic sound quality metrics) based on a fundamental study conducted on an isolated propeller under different isotropic inflow turbulence conditions. In addition, the investigation is extended to different collective pitch angles of the propeller blades.

Section 2 describes the experimental setup employed for the aeroacoustic measurements and the acoustic equipment used. The conventional and psychoacoustic sound metrics used for the characterization are explained in section 3. Lastly, the main results are discussed in section 4, and the conclusions are drawn in section 5.

2. EXPERIMENTAL SETUP

The aeroacoustic measurements of the propeller were conducted at the anechoic, open-jet wind tunnel (A-Tunnel) at Delft University of Technology [15]. The wind tunnel circular outlet (exit diameter of 600 mm) placed on the floor of the facility has a contraction ratio of 15. An additional axisymmetric nozzle with an exit diameter D_{ext} of 420 mm was attached on top of the outlet, see Fig. 1, increasing the overall contraction ratio to approximately 30.

The experiments featured a six-bladed propeller made of steel with a diameter D_p equal to 203.2 mm (8") and a manually adjustable collective pitch angle β. In this study, β values of 25°, 27.5°, 30°, and 32.5° were investigated. This propeller (normally known as X-PROP-S) has been the subject of several publications; for its geometry, including spinner and nacelle dimensions, the reader is referred to [16]. The propeller was placed at a distance of 252 mm ($0.6\,D_{ext}$) from the exit plane of the nozzle. For additional information on the experimental setup the interested reader is referred to [6].

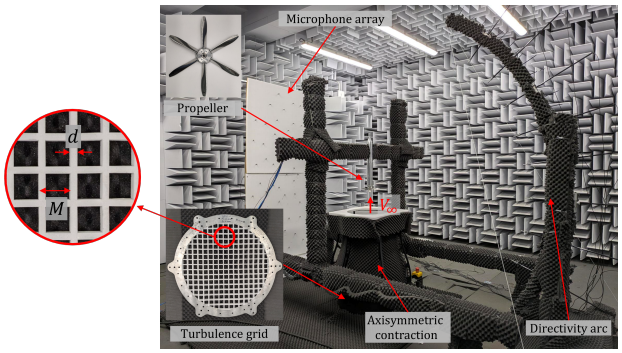

Figure 1: Experimental setup in the A-tunnel.

To investigate different inflow turbulence conditions, three different squared-mesh planar grids made of aluminum plates (thickness 5 mm) were placed at the junction between the axisymmetric nozzle and the wind tunnel outlet, see Fig. 1. The three grids (named A, B, and C) had the same open area ratio of 64% but different values for the bar width d and mesh length M, see Table 1 and Fig. 1. These differences in grid geometries enable various combinations of turbulence intensity TI (defined as the ratio between the root-mean-square velocity fluctuations u'_{rms} and the freestream velocity in the streamwise direction U_∞) levels and streamwise turbulence integral length scales Λ. Table 1 gathers these values for a freestream velocity U_∞ of 30 m/s and a streamwise distance of $x = 0.4\,D_{ext}$ downstream of the nozzle exit. The values for the reference grid-off case are also presented in the same table. All these values were obtained using hot-wire anemometry measurements [6].

Table 1: Bar width d, mesh length M, and turbulence intensity TI for each of the turbulence grids at a distance $x = 0.4\,D_{ext}$ downstream of nozzle exit for U_∞ of 30 m/s [6].

Grid	d, [mm]	M, [mm]	TI, [%]	Λ, [mm]
Off	N/A	N/A	<0.1	N/A
A	7	35	1.97	11.4
B	10	50	2.75	14.1
C	12	60	3.44	16.2

The acoustic measurements were performed using a phased array containing 63 free-field microphones and a directivity arc containing 8 microphones, see Fig. 1, spanning an emission angle range of 70° from $\theta = 70°$ to 140°, with the $\theta = 90°$ corresponding to the rotor disk plane and $\theta = 0°$ to the upstream direction. Both arrays of microphones were positioned at a distance of 1.3 m ($\approx 6.5 D_p$) from the propeller's axis, with the directivity arc centered at the propeller's rotation center. To account for the sound convection due to the flow, the acoustic data recorded was corrected in terms of amplitude and polar emission angle θ, following the guidelines explained in [17]. Therefore, the polar emission angles and amplitudes shown henceforth in directivity plots (Figs. 4-15) already present this correction. A sampling frequency of 51200 Hz and a recording time of 60 s were employed, which corresponds to approximately 10,000 propeller rotations acquired per operating condition.

In order to reduce acoustic reflections, acoustic absorbent materials (melamine and pyramidal polyurethane foam panels) were placed over all exposed surfaces within the anechoic plenum, see light and dark gray surfaces in Fig. 1, respectively. The turbulence grids were also equipped with 20-mm thick melamine foam panels, which were water-jet cut to the respective grid geometry and glued onto the downstream side to suppress both secondary reflections and the generation of tones by vortex-shedding mechanisms [18].

3. CONVENTIONAL AND SOUND QUALITY METRICS

Conventional sound metrics typically used in noise assessment pose challenges for quantifying noise annoyance [9]. Nevertheless, current noise regulations still employ these metrics for enforcing environmental noise laws. Therefore, the current study considers the equivalent sound pressure level $L_{\text{p,eq}}$, as well as the maximum tone-corrected perceived noise level (PNLT) to assess the noise emissions of both propellers. The latter is the base for the effective perceived noise level (EPNL) metric, which is typically employed during aircraft noise certification processes [19].

Unlike the sound pressure level L_{p} metric, which quantifies the purely physical magnitude of sound based on the pressure fluctuations, Sound Quality Metrics (SQMs) describe the subjective perception of sound by human hearing. Hence, SQMs are expected to better capture the auditory behavior of the human ear compared to conventional sound metrics typically employed in noise assessments. The five most commonly-used SQMs [20] are:

- Loudness (N): Perception of sound magnitude corresponding to the overall sound intensity.
- Tonality (K): Perceived strength of unmasked tonal energy within a complex sound.
- Sharpness (S): High-frequency sound content.
- Roughness (R): Hearing sensation caused by modulation frequencies between 15 Hz and 300 Hz.
- Fluctuation strength (FS): Assessment of slow fluctuations in loudness with modulation frequencies up to 20 Hz, with maximum sensitivity for modulation frequencies around 4 Hz.

These five SQMs were calculated for each recording and combined into a single global psychoacoustic annoyance (PA) metric following the model proposed by Di *et al.* [21]. Henceforth, the top 5% percentiles of these metrics (values exceeded 5% of the time) are reported (and hence the sub-index *5*). All the SQMs and the PA metric were computed using the open-source MATLAB toolbox SQAT (Sound Quality Analysis Toolbox) v1.2 [22]. The R and FS metrics evaluate the amplitude modulation and, since the result comparisons are made for the same propeller rotational speed, their variations were not as significant as for the other metrics and are, therefore, not presented in this paper for the sake of brevity.

4. RESULTS

From the different test conditions evaluated, the results presented in this paper correspond to a freestream velocity U_∞ of 30 m/s and a rotational frequency f_r of 166.76 Hz, resulting in a tip Mach number $M_{\text{tip}} = V_r/c_0$ of 0.325, where $V_r = \sqrt{(\pi f_r D_p)^2 + U_\infty^2}$ and $c_0 = 340$ m/s (speed of sound at 16°C).

4.1 Influence of the inflow turbulence intensity

Figure 2 depicts the comparison of the spectra for all grid cases for $\beta = 30°$ and a polar emission angle of $\theta = 140°$, i.e. downstream of the propeller plane. The frequency axis is normalized with respect to the blade passing frequency (BPF $= Bf_r \approx 1$ kHz, where $B = 6$ is the blade count). In general, it is observed that increasing TI causes a substantial raise in the broadband noise up to roughly the 7$^{\text{th}}$ BPF (≈ 7 kHz). On the other hand, a considerable reduction in high-frequency broadband noise is observed for all the grid cases after the 11$^{\text{th}}$ BPF (≈ 11 kHz).

For conciseness, the result comparison of varying turbulence grids in this section is limited here to the cases with $\beta = 30°$, although other collective blade pitch angles presented comparable findings.

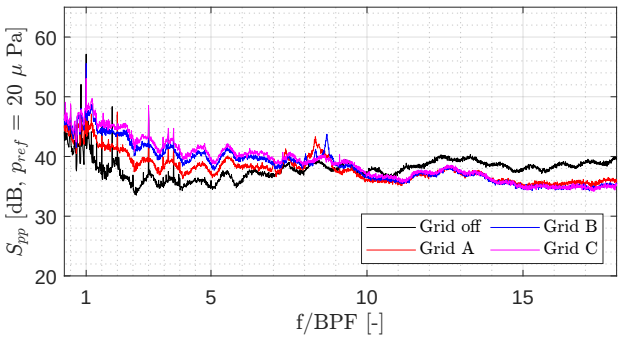

Figure 2: Power spectra S_{pp} of acoustic pressure for $\beta = 30°$ and all grids for $\theta = 140°$ ($\Delta f = 5$ Hz).

The influence of the inflow TI in the propeller far-field noise emissions was evaluated using directivity plots (Figs. 4-9) at the end of this paper for the different sound metrics considered (both conventional and psychoacoustic).

First of all, Fig. 4 depicts an almost omnidirectional (except for an outlier at $\theta \approx 150°$) emission pattern of the $L_{\text{p,eq}}$ metric that is essentially the same for all the four cases. This highlights the fact that this simple metric (lacking any frequency weighting) is not suitable for

making perceptual comparisons [23]. The PNLT_{max} metric (Fig. 5, on the other hand, starts showing larger differences between the four inflow TI cases, with (in general) larger emission values with increasing TI. Overall, larger values and variability are observed for larger polar emission angles θ. Nevertheless, the directivity patterns are not very uniform. Regarding loudness N_5, Fig. 6 presents a more dipole-like radiation pattern typical in propeller applications [6, 10, 11]. Since loudness is (to a certain extent) an energy-based metric, increasing the TI results in higher N_5 values for all emission angles, showing values up to 30% higher than the baseline grid-off case. This is explained by the higher broadband noise levels observed in the mid-frequency range in the spectra of Fig. 2. In terms of sharpness S_5 (see Fig. 7), the radiation patterns are again dipole-like, but in this case, the grid-off case (lowest inflow TI) presents the highest values. This is due to the fact that the sharpness metric employed represents the ratio of high-frequency loudness with respect to the total loudness. High-frequency noise is, in fact, affected by the presence of a turbulence inflow, but rather surprisingly, not by its turbulence intensity. Unexpectedly, its level is greater with a clean inflow and, therefore, the overall sharpness is roughly 10% lower for the cases with higher TI compared to the grid-off baseline. A similar trend (although with a considerably more irregular radiation pattern) is observed for the tonality K_5 (see Fig. 8). In this case, the additional broadband noise observed in the cases with higher TI (see Fig. 2) effectively masks the characteristic tones of the propeller noise signature (BPF and harmonics), providing K_5 values about half the baseline case without inflow turbulence. Finally, the global PA metric (see Fig. 9) combines the results of all SQMs and shows a similar radiation pattern as N_5 (since loudness heavily influences PA [20]). For the larger polar emission angles θ, the estimated psychoacoustic annoyance is up to about 25% higher than for the grid-off baseline case.

4.2 Influence of the collective blade pitch angle

In a similar way as Fig. 2, Fig. 3 compares the far-field noise emissions for all β cases considered when using Grid C and a polar emission angle of $\theta = 140°$. In contrast to the TI variation, increasing β seems to mostly affect the broadband noise emissions for frequencies higher than the 10^{th} BPF, with lower values reported for increasing β. The spectra below that threshold, on the other hand, roughly remained constant for varying β.

The effect of β on the directionality of the different

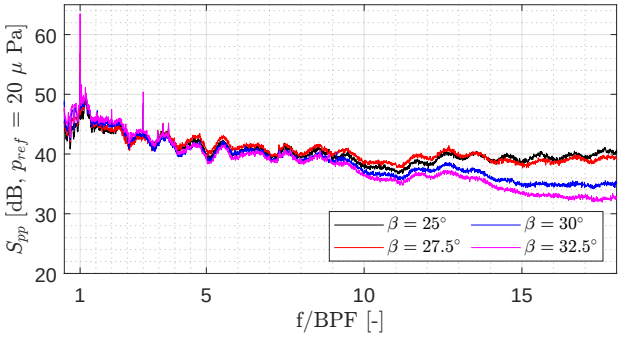

Figure 3: Power spectra S_{pp} of acoustic pressure for Grid C and all β for $\theta = 140°$ ($\Delta f = 5$ Hz).

sound and psychoacoustic metrics for the propeller was evaluated in Figs. 10-15 at the end of this paper. Only the results corresponding to Grid C (i.e. $TI = 3.44\%$) are presented for conciseness, but the conclusions can be extended to other cases.

The results for the $L_{\text{p,eq}}$ metric for this comparison are depicted in Fig. 10, which are essentially the same for all the cases evaluated, like in the TI comparison presented in Fig. 4. In contrast, the PNLT_{max} metric (Fig. 11 presents its largest variations (up to 4 PNTdB) closer to the propeller plane ($\theta \approx 90°$) with higher values for increasing β. This reflects the greater importance of loading noise mechanisms in the propeller's plane, as increasing β results in increased blade loading for a constant inflow velocity and rotational velocity. The loudness radiation patterns presented in Fig. 12 also show this feature, although with a more uniform dipole-like directivity pattern. Near the propeller plane emission angles, differences in N_5 up to 20% are reported, whereas for higher θ values, the results for all cases seem to collapse better. A more consistent variation with β is observed for the sharpness in Fig. 13, where the first two cases ($\beta = 25°$ and 27.5°) follow a very similar trend, but the two higher blade pitch angles present roughly 10% lower S_5 values. This is explained by the aforementioned reduction in high-frequency noise, as seen in Fig. 3. The tonality values for this comparison (with the highly-turbulent Grid C, see Fig 8) are all relatively low, but in the polar plot of Fig. 14, it is observed that the lower β cases present even lower K_5 values (below 0.05 t.u.). Once again, this is likely to be due to the lower masking because of the decrease in broadband noise that these cases present (see Fig. 3). Lastly, the global PA metric presents once again a dipole-like radiation pattern, but with a considerably smaller spread within

the different cases compared to the TI study. In fact, only significant reductions (about 10%) in PA are observed for the smaller β cases close to the propeller disk ($\theta \approx 90°$).

5. CONCLUSIONS

The current manuscript discussed the influence of the inflow turbulence intensity (TI) and the collective pitch angle on the noise emissions of an isolated propeller, evaluated with conventional and psychoacoustic metrics. The experimental data considered was measured using a directivity arc in an aeroacoustic wind tunnel campaign.

In general, it was found that increasing the inflow TI considerably raised the measured values of PNLT_{max} and loudness, whereas, on the other hand, sharpness and tonality decreased. The overall psychoacoustic annoyance metric (PA) roughly followed the same trend as loudness. Overall, larger PA values and variability were observed for higher polar emission angles (i.e. downstream of the propeller plane).

Increasing the collective propeller blade pitch angle β also caused a rise in PNLT_{max} and loudness, but also a moderate increase in tonality. This time, higher variations of these metrics were observed in the propeller plane direction ($\theta \approx 90°$). Conversely, sharpness seemed to decrease for increasing β angles. The combined effect of these changes caused a slight increase of PA with $beta$, but was considerably milder than for the TI comparison.

Future work will involve psychoacoustic listening experiments to confirm the findings in this paper and assess the somewhat contradicting trends between loudness and tonality and sharpness. In addition, applying acoustic imaging to the data recorded by the planar microphone array would also be of interest to localize, if possible, the noise sources responsible for these psychoacoustic features [24].

6. ACKNOWLEDGMENTS

This work is part of the HOPE (Hydrogen Optimized multi-fuel Propulsion system for clean and silEnt aircraft) project, and has received funding from the European Union's Horizon Europe research and innovation programme under grant agreement No. 101096275. Additionally, this publication is also a part of the *Listen to the future* project (project number 20247), a part of the Veni 2022 research programme (Domain Applied and Engineering Sciences). The latter project is granted to Roberto Merino-Martinez and is (partially) financed by the Dutch Research Council (NWO).

7. REFERENCES

[1] R. M. Yupa-Villanueva, R. Merino-Martinez, A. Altena, and M. Snellen, "Psychoacoustic Characterization of Multirotor Drones in Realistic Flyover Maneuvers," in 30th *AIAA/CEAS Aeroacoustics Conference, June 4 – 7 2024, Rome, Italy*, 2024. AIAA paper 2024–3015.

[2] S. A. Rizzi, D. L. Huff, D. D. J. Boyd, P. Bent, H. B., K. A. Pascioni, D. C. Sargent, D. L. Josephson, M. Marsan, B. He, and R. Snider, "Urban Air Mobility Noise: Current Practice, Gaps, and Recommendations," Tech. Rep. NASA Technical Memorandum 83199, NASA, 2020.

[3] S. Schade, R. Merino-Martinez, P. Ratei, S. Bartels, R. Jaron, and A. Moreau, "Initial Study on the Impact of Speed Fluctuations on the Psychoacoustic Characteristics of a Distributed Propulsion System with Ducted Fans," in 30th *AIAA/CEAS Aeroacoustics Conference, June 4 – 7 2024, Rome, Italy*, 2024. AIAA paper 2024–3273.

[4] F. Monteiro, R. Merino-Martinez, and L. T. Lima Pereira, "Psychoacoustic Evaluation of an Array of Distributed Propellers Under Synchrophasing Operation," in 30th *AIAA/CEAS Aeroacoustics Conference, June 4 – 7 2024, Rome, Italy*, 2024. AIAA paper 2024–3321.

[5] F. Ahmed, C. A. Ramos-Romero, A. J. Torija Martinez, and M. Azarpeyvand, "Boundary Layer Ingestion Ducted Fan: Aeroacoustic and Psychoacoustic Insights," in *30th AIAA/CEAS Aeroacoustics Conference (2024)*, (Rome, Italy), American Institute of Aeronautics and Astronautics, June 2024.

[6] L. N. Quaroni, R. Merino-Martinez, F. d. N. Monteiro, and S. S. Kumar, "Collective blade pitch angle effect on grid turbulence ingestion noise by an isolated propeller," in 30th *AIAA/CEAS Aeroacoustics Conference, June 4 – 7 2024, Rome, Italy*, 2024. AIAA paper 2024–3209.

[7] E. Grande, G. Romani, D. Ragni, F. Avallone, and D. Casalino, "Aeroacoustic Investigation of a Propeller Operating at Low Reynolds Numbers," *AIAA Journal*, vol. 60, pp. 860–871, Feb. 2022.

[8] A. J. Torija, C. Ramos-Romero, and N. Green, "Acoustic and Psychoacoustic Characterisation of Unmanned Aircraft Systems as a Function of Vehicle Mass and Flight Procedure," in 30th *AIAA/CEAS Aeroacoustics Conference, June 4 – 7 2024, Rome, Italy*, 2024. AIAA paper 2024–3235.

[9] R. Merino-Martinez, R. M. Yupa-Villanueva, B. von den Hoff, and J. S. Pockelé, "Human response to the flyover noise of different drones recorded in field measurements," in 3rd *Quiet Drones conference, September 8 – 11 2024, Manchester, United Kingdom*, 2024.

[10] R. Merino-Martinez, H. Ben-Gida, and M. Snellen, "Psychoacoustic Evaluation of an Optimized Low–Noise Drone Propeller Design," in 30th *International Congress on Sound and Vibration (ICSV), July 8 – 11 2024, Amsterdam, the Netherlands*, 2024.

[11] K. Heutschi, B. Ott, T. Nussbaumer, and P. Wellig, "Synthesis of real world drone signals based on lab recordings," *Acta Acoustica*, vol. 4, pp. 1–10, October 2020.

[12] T. Sinnige, B. Della Corte, R. de Vries, F. Avallone, R. Merino-Martinez, D. Ragni, G. Eitelberg, and L. L. M. Veldhuis, "Alleviation of Propeller–Slipstream–Induced Unsteady Pylon Loading by a Flow–Permeable Leading Edge," *Journal of Aircraft*, vol. 56, pp. 1214–1230, May–June 2019. DOI: 10.2514/1.C035250.

[13] F. Petricelli, P. Chaitanya, S. Palleja-Cabre, S. Meloni, P. F. Joseph, A. Karimian, S. Palani, and R. Camussi, "An experimental investigation on the effect of in-flow distortions of propeller noise," *Applied Acoustics*, vol. 214, p. 109682, Nov. 2023.

[14] N. S. Jamaluddin, A. Celik, K. Baskaran, D. Rezgui, and M. Azarpeyvand, "Experimental analysis of a propeller noise in turbulent flow," *Physics of Fluids*, vol. 35, p. 075106, July 2023.

[15] R. Merino-Martinez, A. Rubio Carpio, L. T. Lima Pereira, S. van Herk, F. Avallone, M. Kotsonis, and D. Ragni, "Aeroacoustic design and characterization of the 3D–printed, open–jet, anechoic wind tunnel of Delft University of Technology," *Applied Acoustics*, vol. 170, pp. 1–16, June 2020.

[16] N. Van Arnhem, R. De Vries, T. Sinnige, R. Vos, G. Eitelberg, and L. L. M. Veldhuis, "Engineering Method to Estimate the Blade Loading of Propellers in Nonuniform Flow," *AIAA Journal*, vol. 58, pp. 5332–5346, Dec. 2020.

[17] R. Amiet, "Correction of open jet wind tunnel measurements for shear layer refraction," in *2nd Aeroacoustics Conference*, (Hampton,VA,U.S.A.), American Institute of Aeronautics and Astronautics, Mar. 1975.

[18] L. Li, H. Zhu, R. Maryami, X. Zhang, and Y. Liu, "Flow and acoustic characterization of turbulence grids at wind tunnel nozzle exit," *Journal of Sound and Vibration*, vol. 590, p. 118535, Nov. 2024.

[19] R. Merino-Martinez, *Microphone arrays for imaging of aerospace noise sources*. PhD thesis, Delft University of Technology, 2018. ISBN: 978–94–028–1301–2.

[20] G. F. Greco, R. Merino-Martinez, A. Osses, and S. C. Langer, "SQAT: a MATLAB-based toolbox for quantitative sound quality analysis," in 52th *International Congress and Exposition on Noise Control Engineering, August 20 – 23 2023, Chiba, Greater Tokyo, Japan*, International Institute of Noise Control Engineering (I-INCE), 2023.

[21] G.-Q. Di, X.-W. Chen, K. Song, B. Zhou, and C.-M. Pei, "Improvement of Zwicker's psychoacoustic annoyance model aiming at tonal noises," *Applied Acoustics*, vol. 105, pp. 164–170, 2016.

[22] Greco, G. F. and Merino-Martinez, R. and Osses, A., "SQAT: a sound quality analysis toolbox for MATLAB (version v1.0)," May 2023. Accessed in May 2023.

[23] R. Merino-Martinez, R. Pieren, and B. Schäffer, "Holistic approach to wind turbine noise: From blade trailing–edge modifications to annoyance estimation," *Renewable and Sustainable Energy Reviews*, vol. 148, pp. 1–14, May 2021.

[24] R. Merino-Martinez, A. Vieira, M. Snellen, and D. G. Simons, "Sound quality metrics applied to aircraft components under operational conditions using a microphone array," in 25th *AIAA/CEAS Aeroacoustics Conference, May 20 – 24 2019, Delft, The Netherlands*, 2019. AIAA paper 2019–2513.

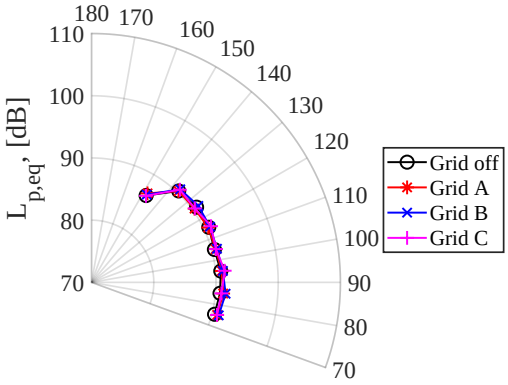

Figure 4: $L_{p,eq}$ directivity for $\beta = 30°$.

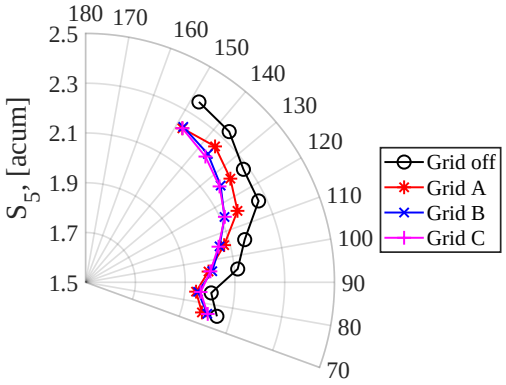

Figure 7: S_5 directivity for $\beta = 30°$.

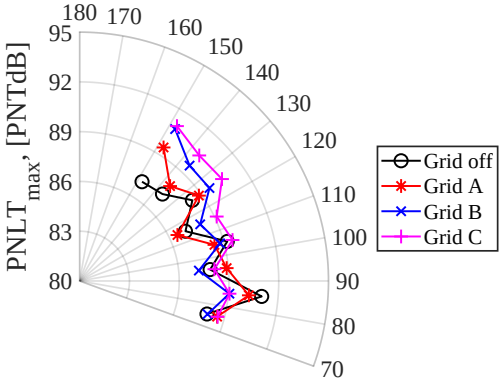

Figure 5: $PNLT_{max}$ directivity for $\beta = 30°$.

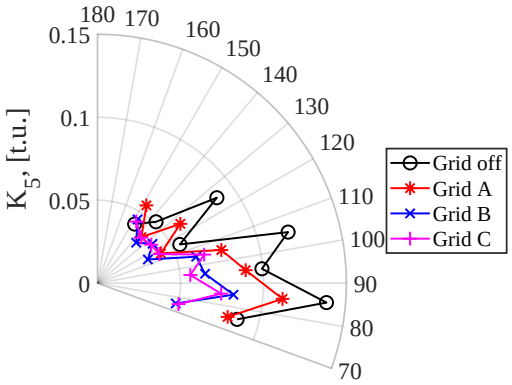

Figure 8: K_5 directivity for $\beta = 30°$.

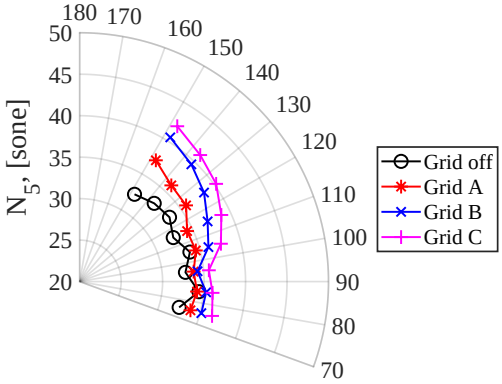

Figure 6: N_5 directivity for $\beta = 30°$.

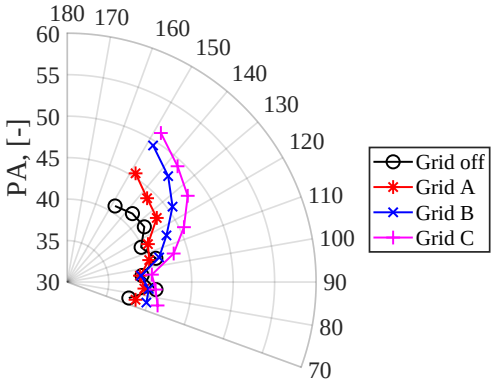

Figure 9: PA directivity for $\beta = 30°$.

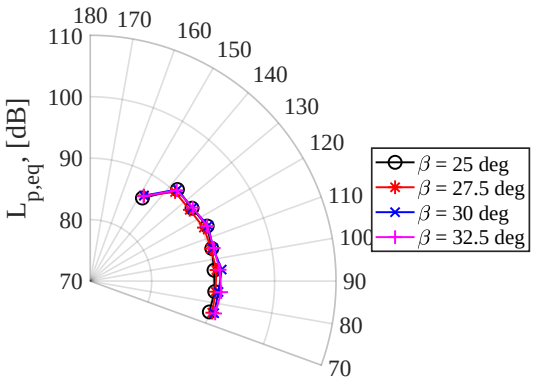

Figure 10: $L_{p,eq}$ directivity for Grid C.

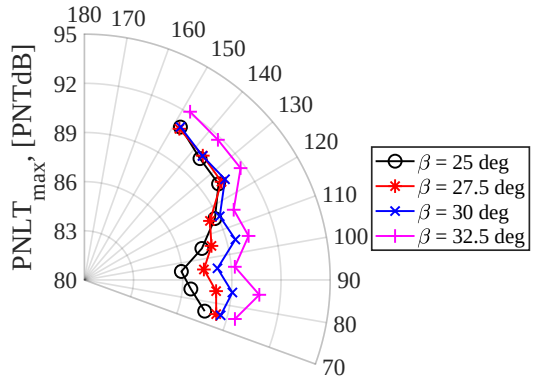

Figure 11: $PNLT_{max}$ directivity for Grid C.

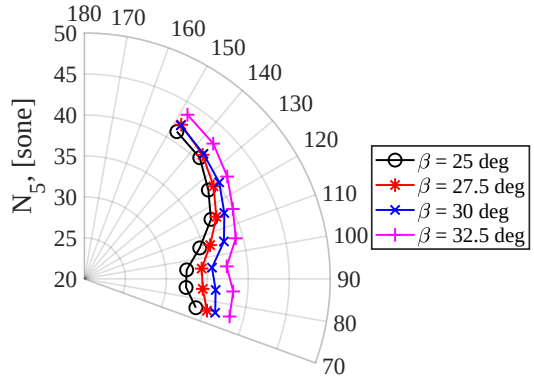

Figure 12: N_5 directivity for Grid C.

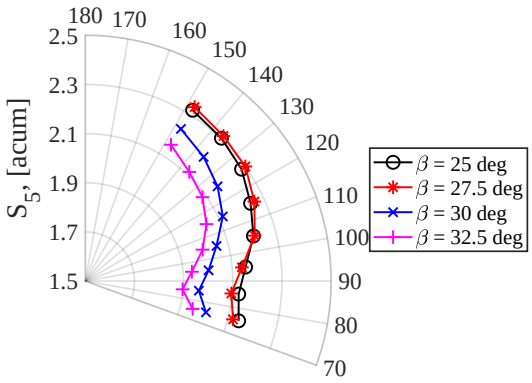

Figure 13: S_5 directivity for Grid C.

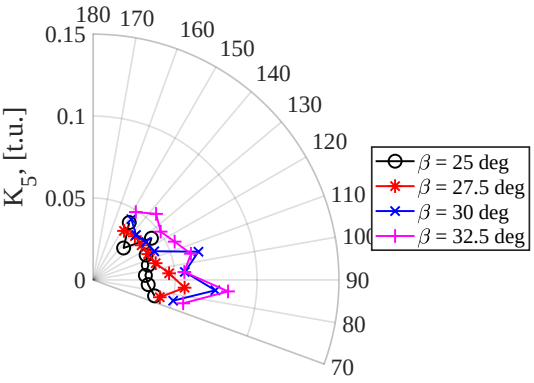

Figure 14: K_5 directivity for Grid C.

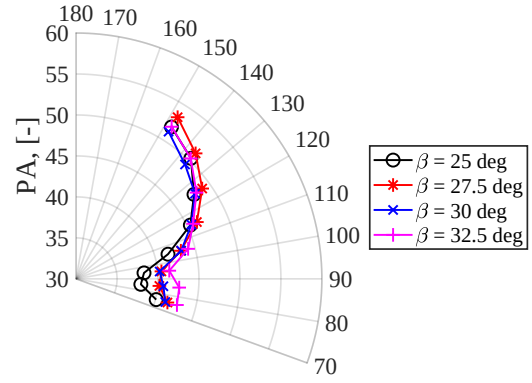

Figure 15: PA directivity for Grid C.